Nanoscale Wettability of Self-Assembled Monolayers Investigated by Noncontact Atomic Force Microscopy

Antonio Checco[†]

Service de Physique de l'Etat Condensé, C.E.A. Saclay, F-91191 Gif-sur-Yvette Cedex, France

Hauke Schollmeyer,[‡] Jean Daillant, and Patrick Guenoun*

Service de Chimie Moléculaire, LIONS, Bât. 125, C.E.A. Saclay, F-91191 Gif-sur-Yvette Cedex, France

Rabah Boukherroub

Institut de Recherche Interdisciplinaire, Institut d'Electronique de Microélectronique et de Nanotechnologie, Cité Scientifique, Avenue Poincaré, B.P 69, 59652 Villeneuve d'Ascq, France

Received May 30, 2005. In Final Form: October 10, 2005

We report on a novel technique to nucleate nanometer-sized droplets on a solid substrate and to image them with minimal perturbation by noncontact atomic force microscopy (NC-AFM). The drop size can be accurately controlled, thus permitting hysteresis measurements. We have studied the nanoscale wettability of several methyl-terminated substrates prepared by the self-assembly of organic molecules. These substrates are alkyltrichlorosilanes on silica, alkylthiols on gold, alkyl chains on hydrogen-terminated silicon, and crystalline hexatriacontane chains on silica. For each of these systems, we report a deviation of the wetting contact angle from the macroscopic value, and we discuss this effect in term of mesoscale surface heterogeneity and long-range solid−liquid interactions.

Introduction

Contact angle measurements are widely used for the evaluation of macroscopic surface characteristics such as wettability, hydrophobicity, adhesion, and the surface tension of solids.[1] Theoretical as well as practical reasons lead to extending such measurements to the nanometer scale. For instance, the contact angle of nanoscale droplets on a given solid is expected to differ from the one measured at the macroscopic scale because of long-range solid−liquid interactions and unsaturated intermolecular interactions at the three-phase contact line.[2] However, the precise magnitude of this effect is still a matter of debate.[3] Beyond solving fundamental issues, the ability to evaluate the wettability of surfaces at small scales is fundamental for applications such as microfluidics.[4]

Atomic force microscopy (AFM), by imaging tiny liquid drops resting on a solid, has the potential to study wetting phenomena on the nanoscale.[5−11] Ideally, AFM operation should be performed under a controlled environment where drops are in actual thermodynamic equilibrium with their vapor phase. This has been rarely achieved in the past because of some obvious technical issues. The most relevant one is the condensation of liquid on the piezoelectric scanner and other electric elements of the AFM that may jeopardize the instrument. Another issue related to AFM imaging under saturated atmosphere is the capillary condensation of a liquid neck between the tip and the sample whenever both come in close proximity,[11,12] a phenomenon strongly interfering with normal operation of the instrument.

In this paper, we present a simple technique that adequately addresses the latter issues, making possible the measurement of the wettability of surfaces at small scales by using volatile liquids. Droplets are condensed on a solid surface and they are imaged in situ by using noncontact AFM[13] (NC-AFM). This imaging technique is able to profile the liquid interface with nanometer-scale resolution without a significant perturbation of the sample. Droplets are formed by nucleation inside a designed cell containing the AFM probe and the sample substrate. The droplet's size is controlled by changing the vapor pressure inside the cell. In particular, because of the high resolution of the AFM, even minimal distortions of the droplet contact line or pinning on surface defects are clearly visible on scales down to tens of nanometers.

The substrates we have investigated comprise four types of methyl-terminated, self-assembled monolayers (SAM): alkyltrichlorosilanes on silica, alkyl chains on hydrogen-terminated silicon, alkylthiols on gold, and hexatriacontane chains on silica. SAM not only provide model systems for wetting studies, but are also widely used systems for surface functionalization.[14]

* To whom correspondence should be sent. E-mail: Patrick.Guenoun@cea.fr.

[†] Present address: Physics Dept., Bldg 510B, Brookhaven National Laboratory, Upton, NY 11973.

[‡] Present address: Materials Research Laboratory, University of California at Santa Barbara, Santa Barbara, CA 93106-5121.

(1) Zisman, W. A. *Contact Angle, Wettability, and Adhesion*, American Chemical Society: Washington, DC, 1964.
(2) de Gennes, P. G. *Rev. Mod. Phys.* **1985**, *57*, 827.
(3) Checco, A.; Guenoun, P.; Daillant, J. *Phys. Rev. Lett.* **2003**, *91*, 186101.
(4) Whitesides, G. M.; Stroock, A. D. *Phys. Today* **2001**, *54*, 42.
(5) Hu, J.; Ogletree, D. F.; Xu, L.; Lio, A.; Salmeron, M. *J. Phys. Chem. B* **1998**, *102*, 540.
(6) Rieutord, F.; Salmeron, M. *J. Phys. Chem. B* **1998**, *102*, 3941.
(7) Xu, L.; Salmeron, M. *J. Phys. Chem. B* **1998**, *102*, 7210.
(8) Fery, A.; Herminghaus, S.; Reims, D. *Ultramicroscopy* **1997**, *69*, 211.
(9) Fery, A.; Pompe, T.; Herminghaus, S. *Langmuir* **1998**, *14*, 2585.
(10) Luna, M.; Colchero, J.; Baro, A. M. *J. Phys. Chem. B* **1999**, *103*, 9576.
(11) Gil, A.; Colchero, J.; Luna, M.; Gomez-Herrero, J.; Baro, A. M. *Langmuir* **2000**, *16*, 5086.
(12) Colchero, J.; Storch, A.; Luna, M.; Herrero, J. G.; Baro, A. M. *Langmuir* **1998**, *14*, 2230.
(13) Martin, Y.; Williams, C. C.; Wickramasinghe, H. K. *J. Appl. Phys.* **1987**, *61*, 4723.
(14) Xia, Y. N.; Rogers, J. A.; Paul, K. E.; Whitesides, G. M. *Chem. Rev.* **1999**, *99*, 1823.

10.1021/la051419b CCC: $33.50
Published on Web 12/03/2005

Despite their importance, these systems have received little attention in past wetting studies using AFM.

This paper is organized as follows. In the first Experimental Section, we describe the AFM nucleation chamber and the settings necessary to image the droplets in the NC-AFM mode. In the second section, we detail our results regarding the nanoscale wettability of the different SAM surfaces by liquid alkanes. In particular, we demonstrate that, although substrates made of alkyltrichlorosilanes on silica or alkyl chains on hydrogen-terminated silicon exhibit a weak chemical heterogeneity, the latter defects affect considerably the contact angle of submicron droplets.

In the case of a surface composed of alkylthiols on gold, the substrate roughness adds up to chemical heterogeneity to control the wettability. The contact line is pinned and a significant contact angle hysteresis is observed. Hexatriacontane monolayers appear to be chemically and geometrically the most homogeneous SAM, but they undergo a partial dissolution when in contact with the wetting liquid.

Experimental Section

Materials. *n*-Alkanes (purity 99%) were purchased from Aldrich and used without any further purification. *n*-Octadecyltrichlorosilane (OTS, $CH_3(CH_2)_{17}SiCl_3$, purity 99%, Fluka) was purified via distillation in a vacuum just before use. Polished silicon wafers with crystalline orientation (111), bearing a native oxide layer, were purchased form Siltronix, France. OTS monolayers were assembled on top of silicon wafers by following the method described by Brzoska et al.[15] Wafers were cleaned by exposure to UV light for 30 min and by immersion in a mixed solution of concentrated H_2SO_4 and 30% H_2O_2 (70:30; v/v) at 150 °C for 30 min. Substrates were successively rinsed with MilliQ water, dried and immersed in a CCl_4/hexadecane (30:70 v/v) solution of OTS with a concentration of 10^{-3} M. The reaction took place at a fixed temperature of 8 °C, well below the critical temperature $T_c = 28$ °C necessary to obtain dense, high quality monolayers.[15] By varying the reaction times, partially and totally grown OTS monolayers were produced. This method is useful to prepare substrates with different chemical heterogeneity.

Alkanethiol monolayers were assembled on top of Au(111) surfaces by 24 h immersion in an ethanol solution (purity 99%, Fluka) of 1-dodecanethiol (DT) with a concentration of 10^{-3} M. Gold substrates were prepared by ultrahigh vacuum (10^{-6} mbar) thermal evaporation onto freshly cleaved mica. The evaporation rate was 1 Å/sec, and the final thickness of the gold layer about 40 nm. To get smoother gold surfaces, we also used the template-stripped technique detailed elsewhere.[16] We deposited a 100-nm-thick gold film onto an oxidized silicon wafer, which acts as a smooth master. Care was taken to carefully clean the silicon with the same procedure described for the OTS coating process. The gold-covered side of silicon wafers was then glued onto another piece of bare silicon by using epoxy glue EPOTEK 377 (Polyscience, USA). After curing the glue in an oven for 30 min at 160 °C, the master was mechanically stripped from the gold layer by using tweezers.

Monolayers of alkyl chains covalently bound to Si(111) were prepared by photochemical reaction of hydrogen-terminated silicon Si(111)−H surface with 1-alkenes.[17] Chains with 16 carbon atoms were used here. The silicon wafers were cleaned in 3:1 concentrated H_2SO_4/30% H_2O_2 at 100 °C for 20 min, followed by multiple rinsing in MilliQ water. Hydrogen-terminated surfaces were obtained by etching silicon wafers with 40% aqueous deoxygenated NH_4F for 15 min. Si(111)H surfaces were transferred under argon into a Schlenk tube containing 10 mL of deoxygenated 1-hexadecene and irradiated in a Rayonet reactor (300 nm) for 3 h. The functionalized substrates were rinsed with pentane, MilliQ water, and trichloroethane.

Table 1. Advancing Contact Angle (θ_{Adv}) and Hysteresis ($\Delta\theta$) of Hexadecane on OTS (Octadecyltrichlorosilane), DT (Dodecanethiol), and AMS (Alkyl Monolayer on Silicon) and Dodecane on C36 (Hexatriacontane Monolayer)

substrate	θ_{adv}	$\Delta\theta$
partial OTS, deg	30	4
complete OTS, deg	43	2
DT on evaporated gold, deg	46	6
DT on ultraflat gold, deg	45	4
AMS, deg	33	3
hexatriacontane, deg	4	1

Self-assembled films of hexatriacontane were prepared as described in detail elsewhere.[18,19] Hexatriacontane (C36) with a purity of 99+% was obtained from Aldrich. Silicon wafers, obtained from Wacker Siltronic GmbH (Burghausen, Germany) with a natural, amorphous ≈15 Å thick oxide layer, were cut into pieces (typically 5 mm × 5 mm) for use as solid substrate. The surfaces (SiO_2) were cleaned with a modified RCA cleaning process (SC-1) as described in ref 20. Onto these smooth surfaces (roughness in the Ångström scale), molecularly thin alkane films were deposited by spin-coating toluene solutions of C36. The solution concentration and the spin-coating conditions determine the overall surface coverage of hexatriacontane. After the evaporation of toluene, the samples were heated to about 80 °C for a few minutes to completely remove the solvent. At this temperature, the C36 melts (interfacial melting point of C36 ≈76.9 °C, bulk melting temperature ≈76.4 °C) and completely wets the substrate surface. The samples are then cooled to room temperature at a rate of about 2 °C/s.

Macroscopic contact angle measurements were performed by using *n*-alkanes ($8 < n < 16$) as test liquids to check the quality of the grafted monolayers.[21] This was carried out under alkane-saturated atmosphere by recording the magnified drop shape with a digital camera. Circle arcs were found to fit well the drop profiles (because the drop size is smaller than the capillary length), and the contact angle was estimated from the fit's parameters with an accuracy of 0.3°. The "tilting plate" method has been used to measure the contact angle hysteresis of the chemically modified surface because it is simple and reliable in case of surfaces with weak heterogeneity.[22] The small contact angles on C36 substrates were measured as follows. Drops were imaged with an optical microscope by using monochromatic light from a Hg lamp ($\lambda = 543.5$ nm). For a drop diameter of $2r$ and a number i of interference fringes, the contact angle θ can be estimated as: $\theta = \sin^{-1}(2rh/r^2 + h^2)$ [$h \approx i\lambda/2n$, n = refractive index (1.45)]. Contact angle measurements are given in Table 1 for all the surfaces studied.

Dynamic Atomic Force Microscopy. Experiments were performed with a M5 AFM system (TM Microscopes, Veeco Metrology Group) in the so-called amplitude modulation mode, i.e., with the cantilever/tip ensemble vibrating at a given drive frequency, close to mechanical resonance. The oscillation amplitude is then affected by the surface forces acting on the tip, which provides a feedback parameter to image the sample topography. This is achieved by scanning the probe while a feedback loop keeps the chosen oscillation amplitude (the setpoint) constant by varying the vertical mean distance between the cantilever and the sample surface. If the cantilever experiences only long-range van der Waals interactions, the imaging is done in the noncontact (NC) mode.[13] If, in addition, the tip touches periodically the surface, thus sampling repulsive and adhesion forces, the imaging mode is called intermittent contact (IC).[23]

However, the oscillating cantilever may switch between the two latter states. To achieve stable NC imaging without any transition

(15) Brzoska, J. B.; Shahidzadeh, N.; Rondelez, F. *Nature* **1992**, *360*, 719.
(16) Stamou, D.; Gourdon, D.; Liley, M.; Burnham, N. A.; Kulik, A.; Vogel, H.; Duschl, C. *Langmuir* **1997**, *13*, 2425.
(17) Boukherroub, R.; Morin, S.; Bensebaa, F.; Wayner, D. D. M. *Langmuir* **1999**, *15*, 3831.
(18) Schollmeyer, H.; Struth, B.; Riegler, H. *Langmuir* **2003**, *19*, 5042.
(19) Merkl, C.; Pfohl, T.; Riegler, H. *Phys. Rev. Lett.* **1997**, *79*, 4625.
(20) Graf, K.; Riegler, H. *Colloids Surf., A* **1998**, *131*, 215.
(21) Ulman, A. *Ultrathin Organic Films: From Langmuir−Blodgett to Self-Assembly*; Academic Press: Boston, 1991.
(22) Krasovitski, B.; Marmur, A. *Langmuir* **2005**, *21*, 3881.
(23) Zhong, Q.; Inniss, D.; Kjoller, K.; Elings, V. B. *Surf. Sci.* **1993**, *290*, L688.

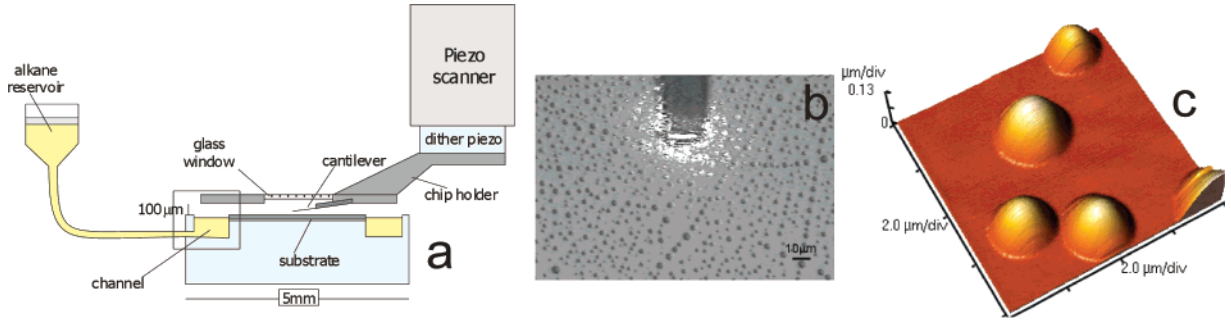

Figure 1. (a) Schematics of the AFM condensation chamber. (b) Optical image showing micron-sized decane droplets condensed on OTS wafer; also shown is the AFM cantilever. (c) NC-AFM picture of decane drops wetting an OTS monolayer.

to the IC mode, it is necessary to use relatively low amplitudes[24−27] (<10 nm) and to choose cantilevers with a high quality factor, which increases sensitivity to weak dispersion forces. It is also suitable to choose probe tips with an apex's size, offering a good compromise between effective volume of interaction and lateral resolution.[28] For this purpose, we used Ultrasharp NCSC12 cantilevers (MikroMasch), whose rectangular 110 μm × 35 μm × 2 μm silicon beams have a natural resonance frequency around 200 kHz, a nominal force constant of 7.5 N/m, and a conic tip long enough (≥15 μm) to minimize acoustic damping effects.[29,30] For these levers, we measured quality factors of about 500 and curvature radii of tips ranging typically between 20 and 50 nm, as measured by scanning electron microscopy. We simultaneously recorded three signals as a function of the (*X, Y*) position of the tip on the plane of the substrate: the vertical displacement of the scanner necessary to keep the amplitude (the height image) constant, the amplitude *A* of the cantilever, and its phase-lag compared to the excitation.

STM Imaging. The surface of gold passivated with dodecanethiol monolayers has been imaged with the same AFM described above used as a scanning tunneling microscope (STM). For this purpose, the silicon tip has been replaced with a conductive tip shaped by cutting platinum−iridium wire with a wire cutter. The tip was biased at +0.3 V with respect to the sample, and a tunneling current of 0.2 nA was used as a feedback signal to image the sample topography.

NC-AFM Imaging of Liquid Structures Condensed from the Vapor Phase. We have saturated the atmosphere surrounding the AFM probe and the sample by designing a special cantilever chip holder (see Figure 1a). The holder has the shape of an aluminum disk of about 5 mm in diameter and a glass window in the center. The cantilever was located at the bottom part of the disk under the window. The window allows measurements of the cantilever bending by the bouncing laser beam technique[31] as well as the observation of the scanned area with an on-line optical microscope. The holder was connected to the AFM piezo-scanner with a small piezo actuator driving the cantilever for operation in dynamic modes. The sample, some millimeters sized, was located on top of a Teflon cylinder of a diameter slightly larger than the cantilever holder (see Figure 1a). A circular channel connected to an external liquid reservoir was machined on the outer part of the cylinder (Figure 1a).

When the AFM cantilever was brought into close proximity with the dry sample surface, the substrate was confined between the cantilever holder and sample Teflon support, which were now separated by several hundred microns. The small volume enclosed by this narrow gap can be rapidly saturated with vapors of a volatile liquid. For this purpose, the circular channel on the sample support was completely filled with a light *n*-alkane (n < 14) until the liquid

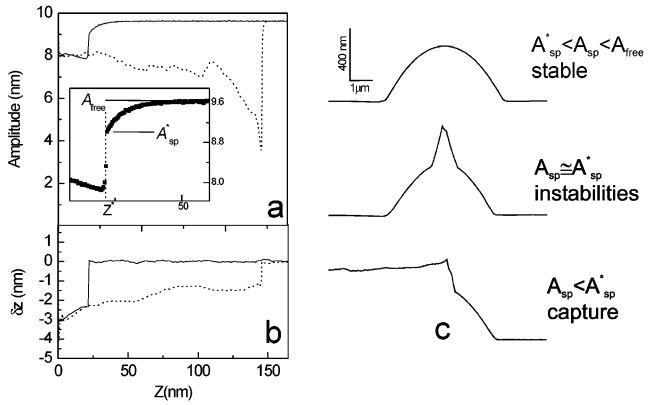

Figure 2. (a) Amplitude, (b) deflection signals recorded while approaching the tip to the free surface of a drop (solid line) and retracting the tip (dotted line); inset in (a) shows a close-up view in the snap-in region. (c) AFM profiles corresponding to different setpoint amplitudes.

wets the sides of the substrate. Under these conditions, the vapor saturated the cell in some tens of minutes. The injection of additional liquid into the channel provided the supersaturation necessary to nucleate many tiny droplets (Figure 1b). The drops grow until the pressure inside the chamber decreased due to condensation; after this they began to evaporate slowly.

The vapor condensed equally on the surface of the silicon cantilever, therefore increasing its mass.[32] This effect induced a negative shift (of about 50 Hz) of the cantilever resonance frequency, which was clearly visible in the frequency spectra under saturated vapor conditions.

Once the droplets have been stabilized, the AFM was set up for imaging in the noncontact mode. This was done by setting a free oscillating amplitude of the cantilever $A_f \cong 10$ nm at a frequency slightly above the resonance $f = f_R + 150$ Hz and a setpoint $A_{sp} \leq A_f$. The tip was gently approached to the surface of a drop, by careful reduction of the setpoint, until a contrasted profile was observed. At this point, the sample was scanned at a speed of 0.5 lines/sec and stable images were obtained as shown in Figure 1c. However, these stable images can be obtained only when the setpoint is larger than a critical value denoted as A^*_{sp}. For setpoint values below A^*_{sp}, instabilities in the topography signal were observed. This is depicted in Figure 2c. For a setpoint such that $A^*_{sp} \leq A_{sp} \leq A_{free}$, a stable drop profile was obtained. When A_{sp} gets close to A^*_{sp}, an instability occurs, visible as a "peak" in the topography signal. As a result, the drop can be dragged by the tip. Further reducing of A_{sp} has more dramatic effects leading to loss of the real sample topography. (cf. Figure 2c).

To get more insight into the nature of the instabilities, we have recorded the amplitude *A* and the mean deflection δz of the cantilever[33] while approaching vertically the surface of a drop (cf. Figure 2a−b).

(24) Garcia, R.; San Paulo, A. *Phys. Rev. B* **1999**, *60*, 4961.
(25) Nony, L.; Boisgard, R.; Aime, J. P. *J. Chem. Phys.* **1999**, *111*, 1615.
(26) Kuhle, A.; Sorensen, A. H.; Zandbergen, J. B.; Bohr, J. *Appl. Phys. A* **1998**, *66*, S329.
(27) Anczykowski, B.; Cleveland, J. P.; Kruger, D.; Elings, V.; Fuchs, H. *Appl. Phys. A* **1998**, *66*, S885.
(28) Hartmann, U. *Phys. Rev. B* **1991**, *43*, 2404.
(29) Leveque, G.; Girard, P.; Belaidi, S.; Solal, G. C. *Rev. Sci. Instrum.* **1997**, *68*, 4137.
(30) Fontaine, P.; Guenoun, P.; Daillant, J. *Rev. Sci. Instrum.* **1997**, *68*, 4145.
(31) Meyer, G.; Amer, N. M. *Appl. Phys. Lett.* **1988**, *53*, 1045.
(32) Thundat, T.; Warmack, R. J.; Chen, G. Y.; Allison, D. P. *Appl. Phys. Lett.* **1994**, *64*, 2894.
(33) This is defined as the difference between the mean vertical position of the cantilever, measured over a cycle, and the position of the lever at rest.

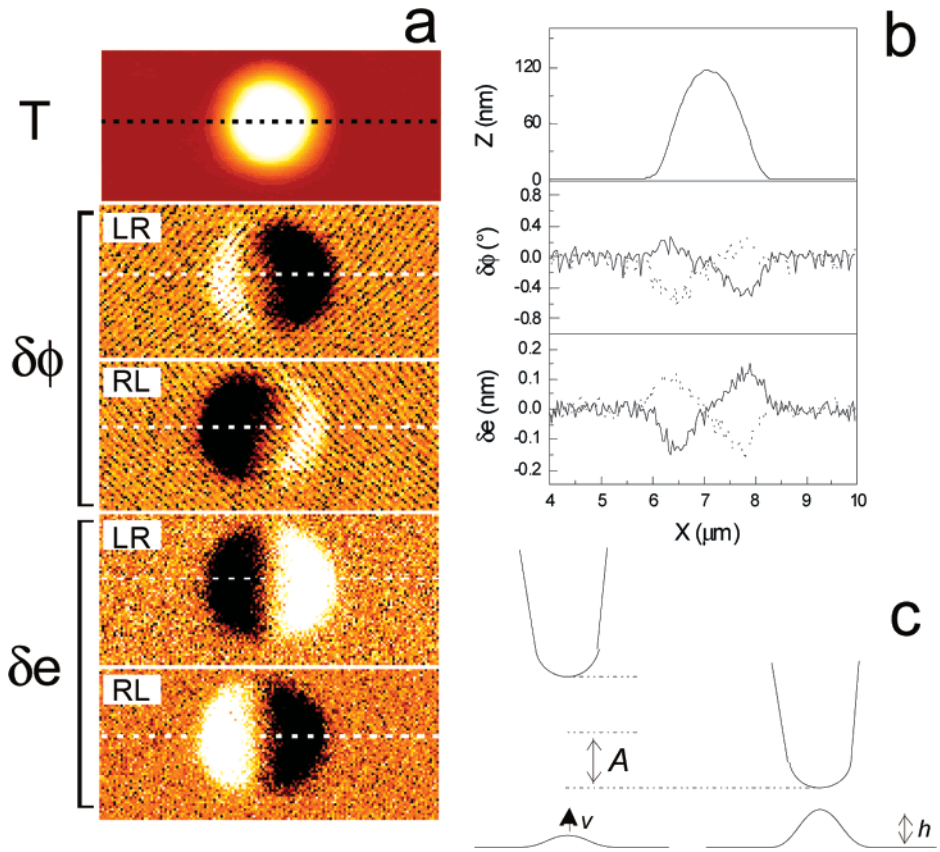

Figure 3. (a) Topography (T), phase shift ($\delta\phi$), and error signal (δe) images of a decane drop on OTS. (b) Corresponding cross-section profiles. (c) Vertical displacement h of the liquid surface induced by the interaction with an oscillating AFM probe.

Far from the liquid (solid line), A was fairly constant, as expected when the tip does not interact with the surface. Thereafter, the amplitude started to decrease over a distance of several nanometers and then it dropped abruptly at a certain point. Beyond this point, labeled as z^* in Figure 2a (inset), a significant deflection of the cantilever toward the surface was also detected (Figure 2b). We explain this behavior as the effect of strong capillary forces arising from the contact between the tip and the liquid surface at the point z^*.

The abrupt decrease of amplitude is due to the energy dissipated by viscous forces associated with the stretching of the capillary bridge connecting the tip and the drop. The amplitude drop induced a fast response of the Z feedback loop, which suddenly increased the vertical mean distance between the cantilever and the sample surface. This caused the rupture of the capillary bridge due to hydrodynamic instability. At this point, the amplitude A_{free} was restored, as visible in Figure 2a (dotted line), and the feedback loop re-approached the tip to the liquid surface to achieve noncontact imaging as before the occurrence of the impact. This explains the "peak" observed in Figure 2c (2nd profile from the top). The complete loss of real topography occurs when A_{sp} was decreased far below A^*_{sp} (Figure 2a), and the Z feedback cannot retract the cantilever far enough from the drop to break the capillary neck. In this case, the drop was dragged on the substrate together with the tip. Conversely, by keeping $A_{sp}{}^* < A_{sp} < A_{free}$ (cf. Figure 2a, inset), one can use long-range forces to image the sample off-contact, thus obtaining stable and meaningful images (cf. Figure 1c).

The presence of capillary forces in NC-AFM imaging was also ruled out by measurements of the power dissipated by the cantilever during the interaction. Because in NC-AFM the cantilever motion stays harmonic to a good approximation,[34] the average power P_{diss} dissipated by the cantilever driven at a frequency f is related to its phase lag φ according to the following expression:[35,36]

$$\bar{P}_{diss} = \frac{\pi k f^2}{f_{res}}\left(A_{fr}A_{sp}\left(\left(\frac{f_{res}}{f} - \frac{f}{f_{res}}\right)^2 + \frac{1}{Q^2}\right)\sin\varphi - \frac{A_{sp}{}^2}{Q}\right) \qquad (1)$$

where A_{sp}, A_{fr} are the setpoint and the free amplitude, respectively, and Q and f_{res} the quality factor and the resonance frequency of the cantilever, respectively. Whenever the tip touches the droplet surface, the onset of capillary forces leads to considerable energy dissipation and, therefore, to strong phase contrast between the drops and the surrounding dry substrate. Indeed a large phase contrast has been observed in tapping mode imaging of liquid drops.[8,9]

However, as shown in Figure 3a, only a little ($\varphi < 1°$) phase difference between dry and wet region of the sample was measured in the regime of stable imaging described above. Moreover, the changes of φ depend on the fast scanning direction X, and they appear correlated with modulations of the error signal, δe (i.e., the difference between the actual oscillation amplitude and the setpoint amplitude, see Figure 3b). This would indicate that the observed phase contrast is not associated with energy dissipation but with changes of A_{sp}, which are not perfectly compensated by the Z feedback loop as the tip encounters surface topography.[37] This happens because of the finite response time of the loop which is set by t_s, the inverse of scanner Z natural frequency, and $t_l = Q/f_{res}$, the transient response of the cantilever.[38] For our system, $t_s \approx t_l \approx 1$ ms, which is comparable to one pixel acquisition time, $t_a = 2$ s/256 = 8 ms. This explains why $\delta e \neq 0$ in correspondence with the slopes of the topography leading to the observed minute phase variations. These observations demonstrate that, in our case, the imaging is performed in the true noncontact mode and the perturbation of the liquid interface is negligible, especially when compared to tapping mode imaging.

The same conclusion can be drawn by estimating the power dissipated during stable NC-AFM imaging according to eq 1, where

(34) Stark, M.; Stark, R. W.; Heckl, W. M.; Guckenberger, R. *Appl. Phys. Lett.* **2000**, *77*, 3293.
(35) Anczykowski, B.; Gotsmann, B.; Fuchs, H.; Cleveland, J. P.; Elings, V. B. *Appl. Surf. Sci.* **1999**, *140*, 376.
(36) Ashby, P. D.; Lieber, C. M. *J. Am. Chem. Soc.* **2005**, *127*, 6814.
(37) Sulchek, T.; Yaralioglu, G. G.; Quate, C. F.; Minne, S. C. *Rev. Sci. Instrum.* **2002**, *73*, 2928.
(38) Landau, L. D.; Lifshitz, E. M. *Mechanics*, 2nd ed.; Pergamon Press: Elmsford, NY,1976.

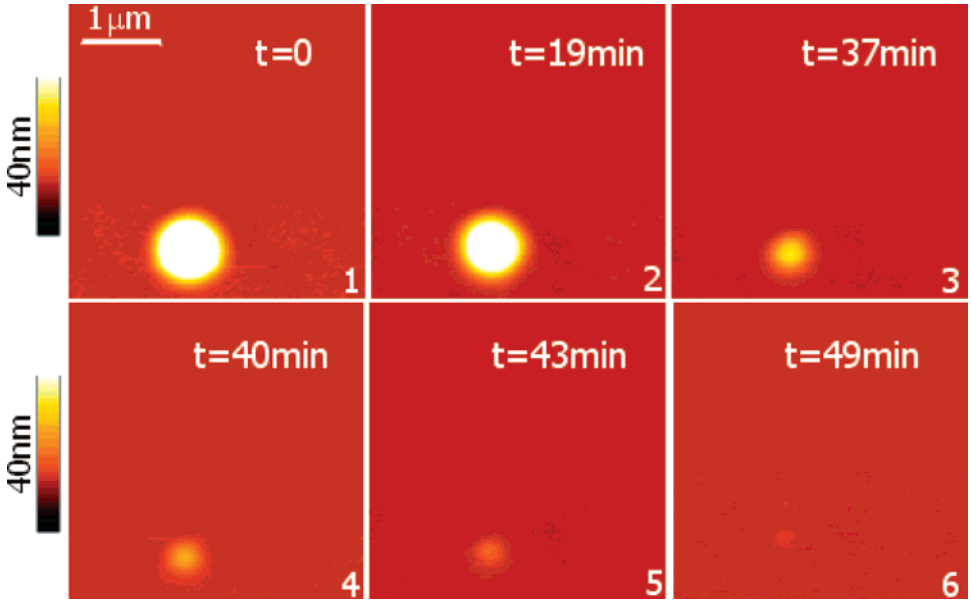

Figure 4. Temporal sequence showing the evaporation of decane drop on OTS surface.

the following numerical values were used (as found in the Experimental Section): $k = 7.5$N/m, $f_R = 200$ kHz, $f_{SP} = f_R + 150$ Hz, $\varphi_{SP} = 120°$, $A_{sp} = 9$ nm, $A_{fr} = 10$ nm, and $Q = 500$. We have obtained $P_{diss} = 0.1$ pW, a rather small value, similar to those reported in ref 35 when the imaging of solid substrates was performed in the attractive regime. As shown in Figure 3a, P_{diss} is similar on the dry and the wet region of the substrate. This also indicates that a negligible power was dissipated through viscous deformation of the drop surface induced by the interaction with the tip. Further, one can show that the vertical, static deformation of the interface, called h in Figure 3c, is small under the conditions of NC-AFM imaging described above. Indeed, h is set by the balance between the disjoining pressure Π due to tip/sample dispersive forces and the capillary pressure in the surface bump.[39] Given the Hamaker constant alkane/silica $H_{alk/SiO_2} \cong 10^{-19}$ J[40] and the average tip/sample separation of several nanometers, (as estimated from Figure 2a inset) we obtained $\Pi \cong 10^5$ Pa and h in the Ångström range.[39]

To conclude this section, we show how it is possible to control the droplet size by changing the vapor pressure inside the chamber. After nucleation and stabilization, the drop size can be reduced either by removing the liquid from the channel reservoir (Figure 1) or by slightly lifting up the cantilever holder, thus opening the cell. In both cases, the vapor pressure inside the cell decreased and droplets evaporated slowly on a time scale long enough (~1 h) compared to the typical image acquisition time (~1 min), as shown in Figure 4. This process can be reversed by re-injecting liquid into the circular channel, which induces recondensation of drops. In this manner, the contact line can be moved in a controllable way, which enables studies of contact line pinning and roughening at small scales.

Results and Discussion

Wetting of OTS Monolayers. In this section, we present the results of our study of wetting of silane monolayers by three light *n*-alkanes ($n = 9, 10, 12$). Completely and partially grown monolayers have been characterized by tapping mode AFM, and the results are shown in Figure 5a, b, d, and e. Image (a) shows the topography of an incomplete OTS surface prepared by 10 min immersion of the substrate in the OTS solution. In the picture, micron-sized fractal islands composed of densely packed alkyl chains are clearly visible. The region between these islands is composed of smaller domains as well as by less dense aggregates of chains about 0.5 nm thinner than the dense regions. In Figure 5b, these more disordered regions of the monolayer show a larger phase contrast compared to that of dense domains, because of their different viscoelastic properties,[35,41] as well as to larger adhesion to the AFM tip.[42−44] A larger adhesion is consistent with alkyl chain disorder because a monolayer exposing equally CH_2 and CH_3 groups has a surface energy larger than that of pure methyl-terminated surfaces.[1] Macroscopic contact angle measurements confirm such observations because the critical surface tension of partial OTS monolayers is found to be $\gamma = 22.5$ mN/m, larger than the one of a well-ordered CH_3 surface,[45] while the contact angle hysteresis is about 4°.

Conversely, an immersion time of 90 min in the OTS solution gives rise to completely formed monolayers with a more uniform phase contrast, as visible in Figure 5d. Such monolayers have rms roughness of 2−3 Å, $\gamma_c = 20.7$ mN/m, and a hysteresis of only 1−2°. These values are typical of uniformly silanized substrates.[1,45]

In the first phase of our study, we have studied the wettability of alkanes on incompletely formed OTS monolayers. The substrate was positioned into the condensation chamber and exposed to saturated vapors of dodecane. AFM images show that liquid condenses as a 5-nm-thick film in the interstitial regions between the dense islands (which now have a negative topographical contrast). This demonstrates that the disordered regions are more wettable than the denser islands. When droplets are nucleated on this substrate, they appear to have a very distorted and pinned contact line crossing both dense and nondense domains, as visible in Figure 5c. We have measured the local contact angle of droplets by fitting circles to the portion of the interface profile close to the contact line. θ varies between 11° and 15°, which is lower than the advancing and receding dodecane contact angles as measured macroscopically, respectively 24° and 20°.

The same procedure as described above but performed on completely formed monolayers gave different wetting behavior.

(39) Dagastine, R. R.; White, L. R. *J. Colloid Interface Sci.* **2002**, *247*, 310.
(40) Israelachvili, J. N. *Intermolecular and Surface Forces*; Boston Academic Press: Boston, 1992.
(41) Tamayo, J.; Garcia, R. *Langmuir* **1996**, *12*, 4430.
(42) VanNoort, S. J. T.; VanderWerf, K. O.; DeGrooth, B. G.; VanHulst, N. F.; Greve, J. *Ultramicroscopy* **1997**, *69*, 117.
(43) Bar, G.; Brandsch, R.; Whangbo, M. H. *Langmuir* **1998**, *14*, 7343.
(44) Noy, A.; Sanders, C. H.; Vezenov, D. V.; Wong, S. S.; Lieber, C. M. *Langmuir* **1998**, *14*, 1508.
(45) Brzoska, J. B.; Benazouz, I.; Rondelez, F. *Langmuir* **1994**, *10*, 4367.

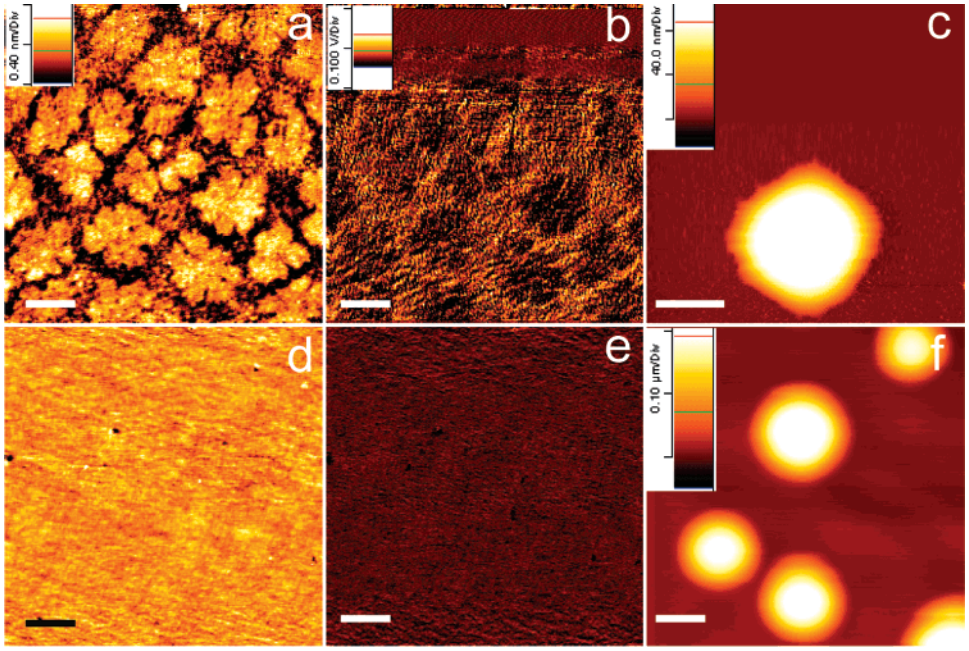

Figure 5. (a) IC-AFM image of a partially grown OTS monolayer, (b) corresponding phase image, and (c) NC-AFM picture of a dodecane droplet condensed on the surface (a). (d) IC-AFM image of a completely grown OTS monolayer, (e) corresponding phase image, and (f) NC-AFM picture of dodecane droplets condensed on the surface (d). For all pictures, the lateral scale bar denotes 1 μm.

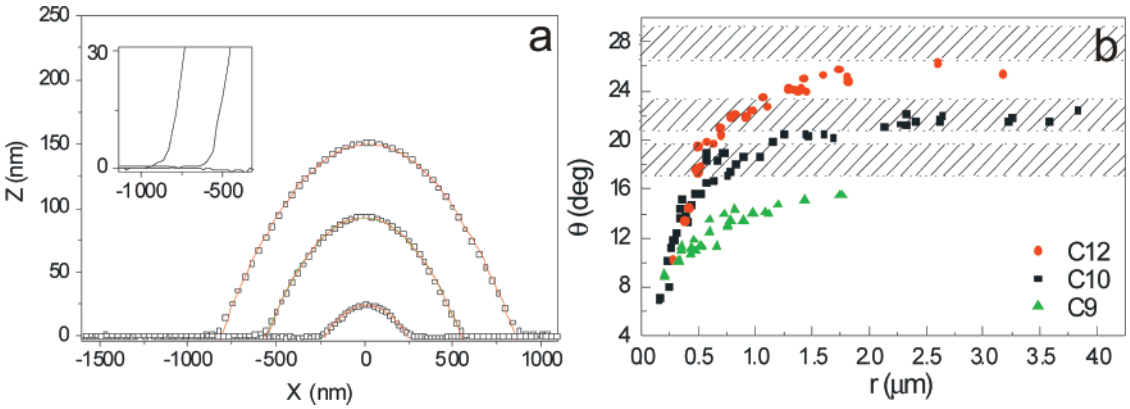

Figure 6. (a) NC-AFM radial profiles (open squares) of decane drops on OTS wafer, fitted with spherical cap shape (continuous lines). Inset shows the smoothed profile near the contact line. (b) Contact angle vs base radius for dodecane (circles), decane (squares), and nonane (triangles).

No film-like condensation was observed on any region of the substrate. Rather, the nucleation of alkane droplets with a circular-shaped contact line is observed as shown in Figure 5f. Droplets are found to have a spherical shape, as expected when gravity effects are negligible. After flattening of the pictures, the droplets were fitted to a spherical cap. The contact angle θ and the base radius r were obtained from four different cross-sections of each drop (cf. Figure 6a). Note that, in the fit, we have excluded points close to the contact line where the drop profile appears smoothed due to tip/sample geometry convolution and to the finite response time of the Z feedback loop. The accuracy of the measurement is limited by tip/sample convolution and scanner nonlinearities. By using numerical techniques[46] and assuming a tip curvature radius less than 50 nm, we have estimated the convolution error to be 0.1° for a droplet radius of 1 μm and 0.5° for a radius of 100 nm. This error is small because the curvature radii of all measured droplets are in the micron range, considerably larger than the radius of the AFM probes. Errors associated with piezo nonlinearities are minimized in our AFM by an optical closed-loop control of the scanner's movements.[47]

We have allowed the droplets to evaporate slightly and then measured the size dependence of the contact angle. Results for three alkanes are shown in Figure 6b, where the hatched region denotes values of the contact angle included between advancing and receding angles as measured macroscopically on the OTS surface. The contact angle of largest drops was found to be comparable to macroscopic values, while for the smallest drops, a significant reduction of the contact angle is observed. By increasing and then decreasing the volume of drops as described previously, we have checked that this effect is not due to an enhanced contact line pinning at the nanometer scale. Increasing the volume of a micron-sized decane drop through condensation gives a rather constant contact angle of 21.1°, while letting the drop slightly evaporate gives a contact angle of 20°. This result is compatible with the small values of contact angle hysteresis ($\cong$1°) observed macroscopically. The same measurement carried out on a nanosized drop gives a similar result, which means that the contact line pinning does not increase considerably at small scales.

(46) Keller, D. *Surf. Sci.* **1991**, *253*, 353.

(47) Barrett, R. C.; Quate, C. F. *Rev. Sci. Instrum.* **1991**, *62*, 1393.

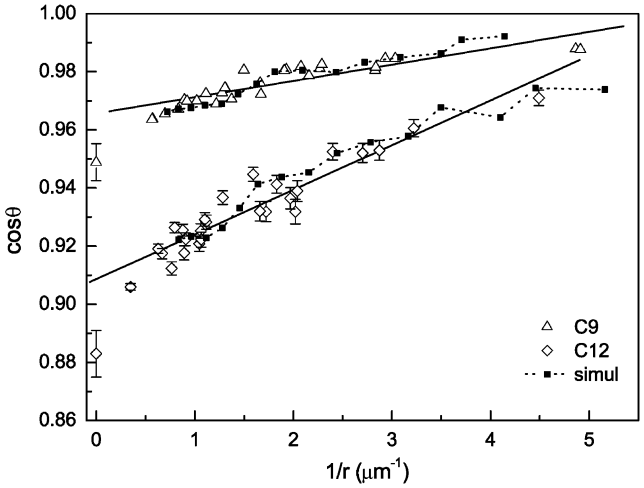

Figure 7. Cosine of the contact angle vs inverse of base radius for nonane (triangles) and dodecane (diamonds) on OTS wafer. Squares and dotted lines represent a numerical simulation of the data performed as explained in the text.

At this point, we have to stress that the dependence of the contact angle upon the drop size has already been observed previously for much larger droplets on substrates of different characteristics.[48−51] To explain the observed decrease of wetting angle at small scales, several effects have to be taken into account. First, the intrinsic energy of the triple line, or line tension τ, can be considered to be at the origin of the observed size dependence of the contact angle. Theory predicts both positive and negative values of τ in the range of $10^{-11}-10^{-12}$ N.[52−54] If one takes into account the line energy, the contact angle is given by the so-called ''modified Young equation'':[55]

$$\cos\theta = \cos\theta_{\mathrm{Y}} - \frac{\tau}{\gamma}\frac{1}{r} \qquad (2)$$

where θ_{Y} is Young's angle for macroscopic drops and r is the base radius of spherical drops. Note that this equation applies in principle to ideally flat and homogeneous surfaces. Equation 2 predicts a simple linear relationship between $\cos\theta$ and $1/r$. The experimental data are plotted in the plane ($\cos\theta$, $1/r$), as shown in Figure 7, where values at $1/r = 0$ correspond to contact angle measurements on millimiter-sized drops under alkane-saturated atmosphere. For all alkanes, a linear fit does not satisfactorily describe the data. This disagreement is particularly apparent because the fit must comply with values of the contact angle at the origin. In any case, the values of τ deduced by the (badly) fitted slope are in the -10^{-10} N range. This is the same order of magnitude as that found by Law et al.[48] for the wetting of octane on silanized substrates and by Pompe and Herminghaus[56] for wetting situations different from the present one.

For our system, the line tension contribution coming from long-range solid−fluid interactions is known to be purely dispersive.[1] This allowed us to estimate the magnitude and the sign of τ in the framework of density functional theory.[54] Phenomenological approaches would not give very different results,[54,57] and details of the calculation have been reported elsewhere.[3] With this approach, negative values of τ in the 10^{-12} N range are obtained that are 2 orders of magnitude smaller than the values found experimentally. For this reason, it is difficult to describe our data in terms of line tension effects only.

Even on fully covered substrates, defects remain between densely packed domains. These defects correspond to disordered regions of the monolayer that are totally wet by alkanes. In a plausible scenario, droplets are nucleated on the highest energy defects and then grow preferentially on the more wettable areas of the substrate. Defects are visible on high-resolution IC-AFM images of the dry substrate as depressions of 0.2−0.5 nm below the dense regions, with a phase shift higher than the rest on the substrate (Figure 8a, b). As explained above, this is due to the larger interaction of the AFM tip on areas of higher surface energy.[43,44]

Accordingly, one can see in Figure 8c that the contact line is not perfectly circular but adopts different distorted configurations depending on the local spatial distribution of defects (compare line 2 and 3 of Figure 8c).[58,59] This small contact line fluctuation along with the minimal pinning observed correspond to the case of weak heterogeneities as discussed by Joanny and De Gennes.[58] The next step is to show how those heterogeneities give rise to the observed decrease of θ at small scales. In ref 3, we have presented a simple model that makes use of AFM images such as that of Figure 8d to define maps of surface defects. "Thresholding" and binarization allows one to determine the portion of the substrate that is likely to be associated with defects. In Figure 8d, defects are represented by black regions where the local contact angle is assumed to be zero (complete wetting). We have calculated the equilibrium contact angle of a droplet, with a fixed volume resting on a certain position of the "binary" surface through numerical minimization of the droplet free energy. This calculation takes into account the spatial dependence of the spreading parameter due to surface chemical heterogeneity (as represented in Figure 8d), while the surface is considered ideally flat. We calculate the equilibrium base radius and contact angle of a large (2000) number of droplets randomly placed on the substrate. To retain only the most favorable nucleation sites, we then calculate the average of the 50 smaller contact angle values. By repeating this calculation for several drop volumes, the size dependence of contact angle can be simulated. Although contact line distortion is not accounted for in the calculation, this simple approach gives results in reasonable agreement with the experiment (see Figure 7) for both nonane and dodecane. Our results show that residual imperfections of the substrate can have a strong influence on small-scale wetting, a crucial effect for practical applications.

Besides the observations described above, the wettability of OTS monolayers nanopatterned by AFM lithography was also investigated. The AFM tip was used to mechanically remove the OTS layer from the silicon oxide. As a result, channels hundreds of nanometers wide and 0.5−3 nm deep were produced, as shown in Figure 9a. These channels are expected to be more wettable than the bare OTS layer because the methyl termination of the OTS monolayer is locally altered by exposing CH_2 groups or even the underlying silicon dioxide. This can be seen again in the phase images recorded simultaneously to topography in the IC-AFM mode. In Figure 9a, two arrays of channels with different depth and spatial periodicity are shown. When these nanostructured surfaces are exposed to saturated dodecane vapors, liquid

(48) Wang, J. Y.; Betelu, S.; Law, B. M. *Phys. Rev. Lett.* **1999**, *83*, 3677.
(49) Drelich, J.; Miller, J. D.; Good, R. J. *J. Coll. Interface Sci.* **1996**, *179*, 37.
(50) Drelich, J. *J. Adhes.* **1997**, *63*, 31.
(51) Drelich, J. *Colloids Surf., A* **1996**, *116*, 43.
(52) Harkins, W. *J. Chem Phys.* **1937**, *5*, 135.
(53) Rowlinson, J. S.; Widom, B. *Molecular Theory of Capillarity*, Clarendon: Oxford; 1982.
(54) Bauer, C.; Dietrich, S. *Eur. Phys. J. B* **1999**, *10*, 767.
(55) Boruvka, L.; Neumann, A. W. *J. Chem. Phys.* **1977**, *66*, 5464.
(56) Pompe, T.; Herminghaus, S. *Phys. Rev. Lett.* **2000**, *85*, 1930.
(57) Dobbs, H. T.; Indekeu, J. O. *Physica A* **1993**, *201*, 457.
(58) Joanny, J. F.; De Gennes, P. G. *J. Chem. Phys.* **1984**, *81*, 552.
(59) Robbins, M. O.; Joanny, J. F. *Europhys. Lett.* **1987**, *3*, 729.

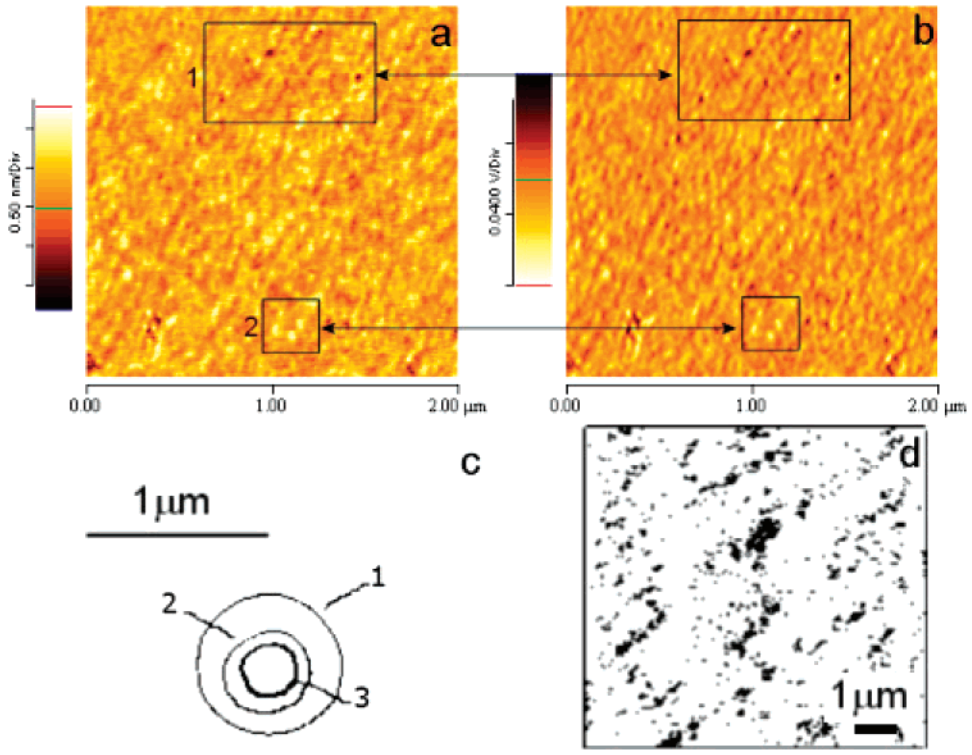

Figure 8. (a) IC-AFM topography of a OTS monolayer and (b) corresponding phase image (note that Z scale is inverted here). (c) Contact line configurations (from 1 to 3) of a decane droplet on OTS recorded during evaporation. (d) Example of thresholding of an OTS picture.

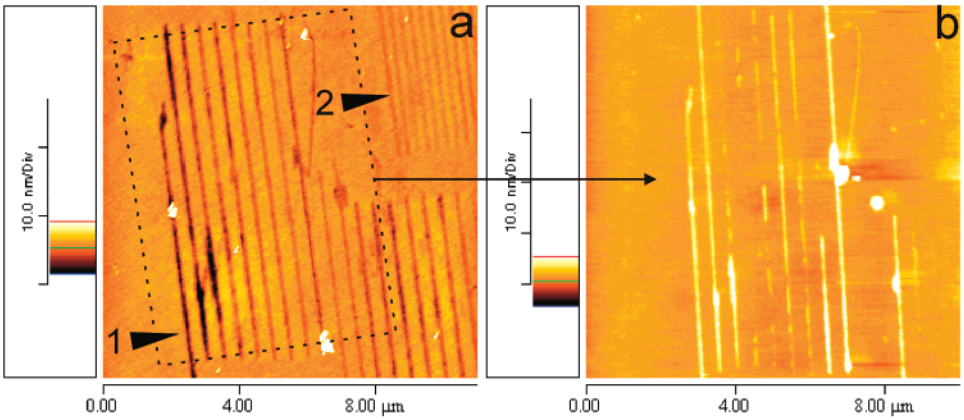

Figure 9. (a) Array of channels with different periodicity written on OTS by using an AFM tip and (b) condensation of dodecane on this patterned surface.

is clearly seen to wet completely some channels while others appear only partially filled. This happens because the removal of the OTS monolayer by scratching is not uniform. Such images clearly demonstrate the ability of NC-AFM to test the functionality of nanofluidic chips or, for example, to study liquid transport phenomena in nanochannels.

Wetting of Alkyl Monolayers on Silicon. In this section, we present, for comparison, results concerning the wettability of alkyl monolayer with 16 carbon atoms, covalently bound onto silicon (shortly AMS). From the AFM images, these monolayers show a steplike structure similar to that observed for the underlying Si(111) (see Figure 10a). The step height of 0.3 nm is in agreement with the distance between adjacent Si(111) atomic planes. This indicates the uniform coverage of the Si surface by the monolayer. The triangular pits visible in the pictures result from the presence of oxygen in the NH_4F solution during the Si etching.[60] The overall roughness of the monolayers measured on the micron scale is typically ~2 Å, while the macroscopic advancing/receding contact angles of hexadecane were found to be 33° and 30° (±0.3°), respectively. These values are slightly lower than those reported by Chidsey et al.[61] in the case of monolayers with 16 carbon atoms and even lower than the ones measured on a dense methyl surface. This result suggests that these AMS are less dense than OTS or DT.

Dodecane micro- and nanodroplets condensed on AMS have a nearly spherical shape (see Figure 10b) and a small contact angle hysteresis comparable to macroscopic values (1−2°). We have also observed, similarly to the case of OTS, a reduction of the contact angle vs the size of drops shown in Figure 11a. For the largest drops, the angle is close to macroscopic values, but it decreases to almost 10° for submicron droplets. A fit of our data according to eq 2 gives $\tau/\gamma \cong -17$ nm or $\tau \cong -10^{-10}$ N (Figure 11b). However, because the physicochemical composition

(60) Wade, C. P.; Chidsey, C. E. D. *Appl. Phys. Lett.* **1998**, *72*, 133.

(61) Linford, M. R.; Fenter, P.; Eisenberger, P. M.; Chidsey, C. E. D. *J. Am. Chem. Soc.* **1995**, *117*, 3145.

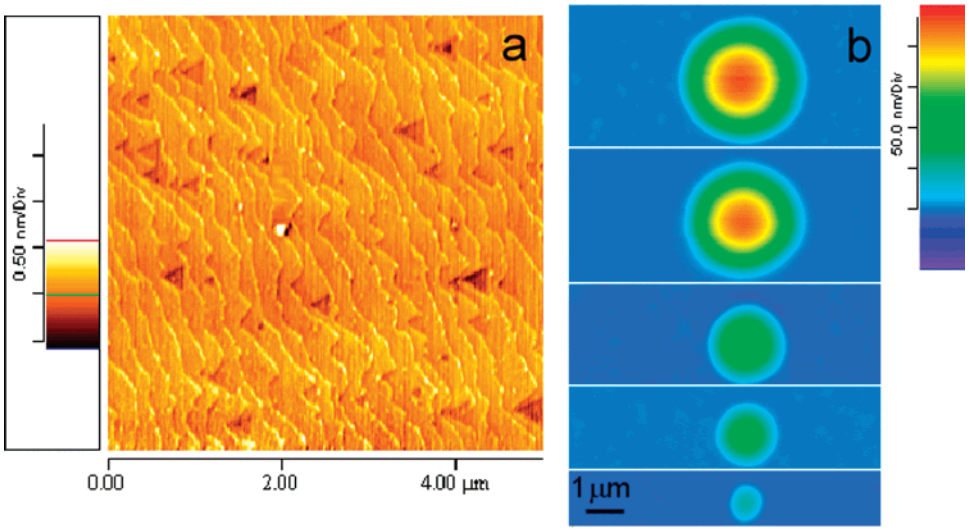

Figure 10. (a) IC-AFM image of an alkyl monolayer (with 16 carbon atoms) bound onto a Si (111) surface and (b) NC-AFM images of dodecane drops condensed on this surface.

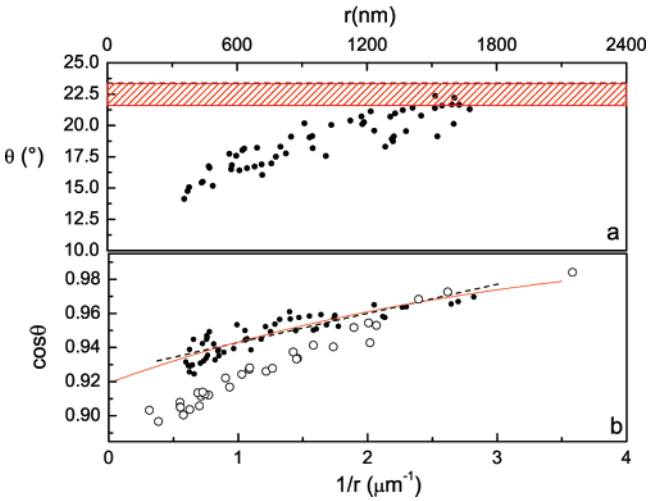

Figure 11. (a) Contact angle vs base radius for dodecane on alkyl monolayer on silicon; the dashed area denotes contact angles measured macroscopically. (b) Same data as in (a) represented in the plane (cos θ, 1/r) (filled dots) and comparison with the dodecane data on OTS (open circles).

of AMS surfaces is very similar to OTS-coated silicon, one could expect theoretically a line tension in the range of some pN. Therefore, we conclude that the mesoscale heterogeneity of the monolayer surface is also responsible for the observed effect. This heterogeneity could be related to variation in the density and in-plane order of the alkyl chains forming the monolayer. For the future, we suggest studying systematically the effect of the monolayer order on the amplitude of contact angle reduction at small scales. This can be done by preparing monolayers with increasing density.

Wetting of Dodecanethiols Monolayers. Dodecanethiol monolayers appear to be considerably rougher than OTS monolayers due to the grainy structure of the underlying gold film. The AFM and STM images (respectively, Figure 12a and 12a inset), suggest that gold evaporated on mica at room temperature is made of about 50-nm-sized grains with a flat top decorated with atomically flat terraces. The roughness of the film is about 4 nm. Contact angle measurements for hexadecane give $\theta_{adv} = 46°$ and $\theta_{rec} = 40°$ for the advancing and receding angle respectively, which is typical for dense monolayers with exposed methyl groups.[62] AFM pictures of "ultraflat" gold samples acquired in the tapping mode also show a grain-like

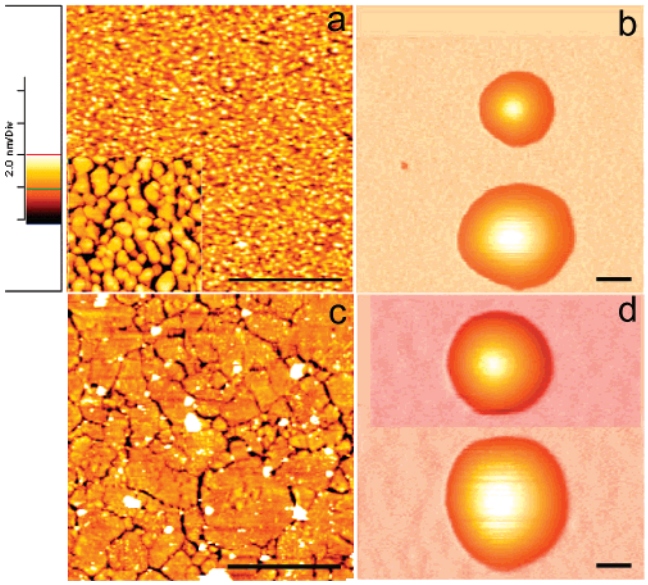

Figure 12. (a) IC-AFM topography of a gold monolayer thermally evaporated on an oxidized silicon wafer then passivated with dodecanethiols. Inset shows a 400-nm-sized detail of the same surface acquired by using STM. (b) NC-AFM images of dodecane droplets condensed on the surface (a). (c) IC-AFM topography of a ultraflat gold surface passivated with dodecanethiols. (d) NC-AFM images of dodecane droplets condensed on the surface (c). For all pictures, the lateral scale bar denotes 1 μm.

structure, but the grain size is considerably larger than the one observed for thermally evaporated gold (Figure 12c). The overall rms roughness as measured by AFM is of the order of 1 nm. The measured advancing and receding contact angles on these surfaces are, respectively, $\theta_{adv} = 45°$ and $\theta_{rec} = 41°$, with a hysteresis sensibly lower than the one found on grainy gold substrates. This result, in agreement with observations reported by other groups,[62,63] indicates that the contact angle hysteresis on alkanethiol monolayers is directly related to the roughness of the underlying gold film.

We have condensed and imaged dodecane microdrops on grainy DT monolayers, and some typical AFM pictures are shown in Figure 12b. In contrast to the wetting behavior observed on

(62) Bain, C. D.; Troughton, E. B.; Tao, Y. T.; Evall, J.; Whitesides, G. M.; Nuzzo, R. G. *J. Am. Chem. Soc.* **1989**, *111*, 321.
(63) Abe, K.; Takiguchi, H.; Tamada, K. *Langmuir* **2000**, *16*, 2394.

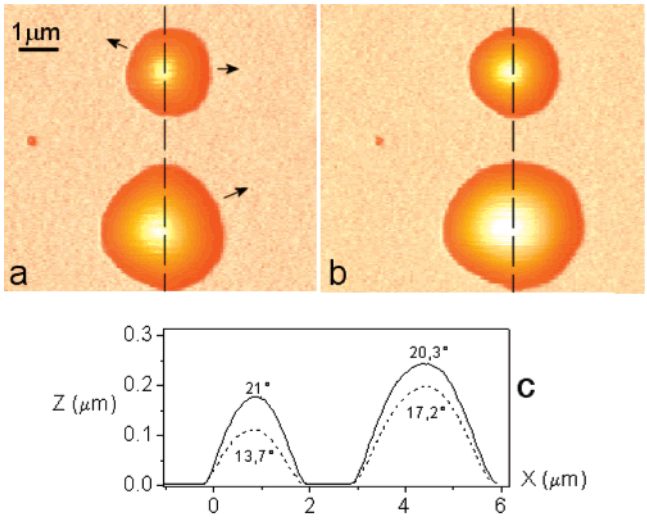

Figure 13. (a) NC-AFM pictures of dodecane droplets on a DT monolayer assembled on top of thermally evaporated gold. (b) Upon increasing the volume of drops, only certain portions of the contact line move while others stay pinned. (c) Radial profiles of drops before (dash line) and after (solid line) the process have been fitted with spherical caps to estimate the contact angle hysteresis.

the complete OTS monolayers, the droplets show a significantly distorted contact line, with a local contact angle varying over the range of several degrees. The pinning of the line is evident upon increasing the drop's volume: the line advances with stick-slip motion, as visible in Figure 13a, b. For each drop, we have measured the contact angle and base radius averaged over eight radial profiles, and the results are plotted in Figure 14a. Data are scattered over about 7°, and no systematic dependence of θ on r can be evidenced. It is worth noting at this point that the maximum advancing contact angle measured here does not exceed 22°, while macroscopically, we have observed values up to 33°.

Such a discrepancy can be explained in different ways. First, because the system shows a large hysteresis, the actual advancing angle of the drops is more difficult to measure. Indeed, the contact line moves with a stick-slip motion and can end up in a metastable state after a jump, not necessarily corresponding to the maximum contact angle. Also, our observations cannot be explained within the classical Wenzel approach.[64] Indeed, the roughness of the gold surface, as obtained from Figure 12a inset, is $r \cong 1.3$ (defined as the ratio of the actual solid area over its projected one), and the macroscopic Wenzel law would predict complete wetting in our case. This failure is not surprising because our droplets have a size close to the characteristic length scale of the surface roughness. The actual contact angle of drops can be evaluated only by taking into account the full wavelength spectrum of the surface roughness.

Another explanation for the observed effect involves the condensation of alkane vapors into the pores between gold grains while the flat grain surface remains dry (cf. Figure 12a inset). In this picture, the micron-sized drops nucleate and grow on a partially wet surface. According to the macroscopic Cassie law,[65] the apparent contact angle of these drops should be smaller than the one measured on a dry substrate. But once again, the use of concepts strictly valid in the case of macroscopic drops is questionable here because the size of our droplets is close to the characteristic length scale of the surface roughness.

To better understand the effect of the substrate roughness, we have studied DT monolayers assembled on "ultraflat" gold. On

(64) Wenzel, R. N. *Ind. Eng. Chem.* **1936**, *28*.
(65) Bico, J.; Tordeux, C.; Quere, D. *Europhys. Lett.* **2001**, *55*, 214.

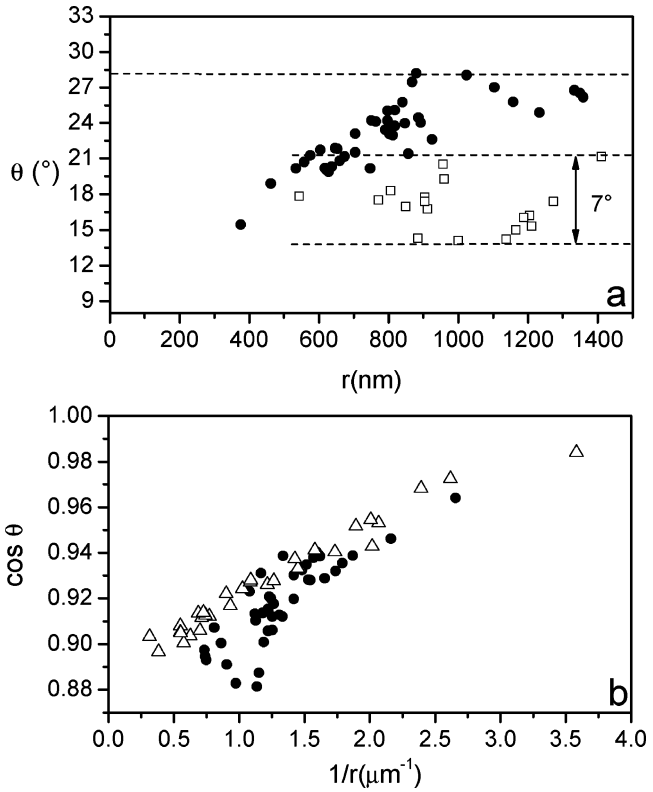

Figure 14. (a) Contact angle vs base radius for dodecane on DT monolayers assembled on thermally evaporated gold (open squares) and on ultraflat gold (filled circles). (b) Cosine of the contact angle vs inverse of base radius for dodecane on ultraflat DT (triangles) and comparison with dodecane data on OTS (open triangles).

these substrates, the alkane drops adopt a more symmetrical shape with a less distorted and pinned contact line. However, occasionally, we have also observed asymmetric drops, as shown in Figure 12d. In Figure 14a, the contact angle of a series of regular drops as a function of the base radius is shown. In contrast with previous observations, the maximum contact angle measured here, about 29°, is close to the macroscopic values measured on the same substrate $\theta_{adv}/\theta_{rec} = 33°/29°$. One can also notice that θ decreases considerably with decreasing the drop size, which is similar to the case of OTS.

By plotting the data in the plane (cos θ,1/r) and fitting them according to eq 2, one obtains $\tau/\gamma \cong -30$ nm or $\tau \cong -10^{-10}$ N (cf. Figure 14b). However, as explained above, the only effect of purely dispersive forces cannot give rise to a line tension larger than some pN. Again the role of the substrate's defects provides a more realistic explanation for the observed behavior. This heterogeneity is evident, not only from the observation of slight asymmetric droplets, but also from IC-AFM inspection of the dry monolayer substrate. Pits, around 1 nm deep, are visible in the sample topography, and their distribution over the substrate is not uniform. These pits are possibly regions where the thiol molecules did not bind to gold, possibly due to the local presence of contaminants originally present on the silicon master and left over after its removal. These surface heterogeneities are also revealed by the phase images due to their large contrast.

Wetting of Hexatriacontane Monolayers. In the next part, the wettability of silicon wafer coated with a thin layer of C36 was studied. These SAMs are characterized by a good short-scale molecular order[18] and by an amount of large-scale structural defects depending on the sample coverage. However, these monolayers are less robust than a covalently bound SAM because

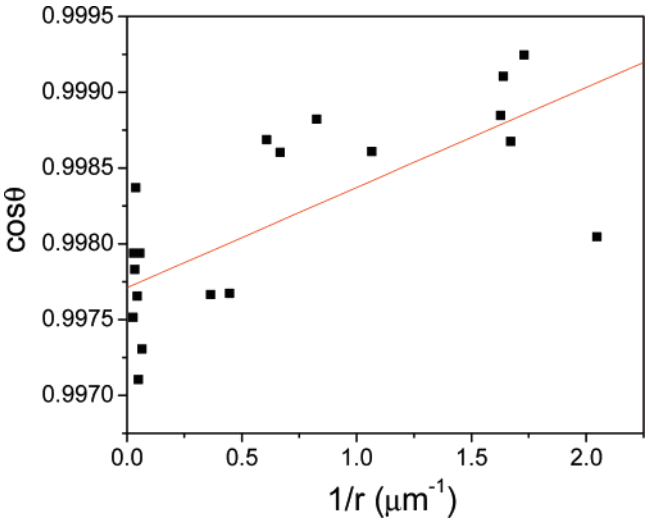

Figure 15. Cosine of the contact angle vs inverse of base radius for drops of dodecane on C36 surface; the straight line is a best fit to the experimental data.

the constituent molecules are not chemically linked to the substrate. Optical measurements (see Table 1) show that dodecane wets C36 monolayers, with a small contact angle between 2° and 4°. Such a low value of θ is not compatible with a dense, methyl-terminated surface. This result can be explained by a partial dissolution of the initial, dense C36 monolayer when in contact with the bulk liquid dodecane. In this respect, the interpretation of the experimental data is more complicated than that for cases discussed before. In Figure 15 are reported contact angle data vs drop size for dodecane on C36 substrate. Only a slight dependence of θ on the droplet's size can be evidenced, leading to an apparent line tension of $1.3 \pm 0.3 \times 10^{-11}$ N. This value, an order of magnitude less than that found for the silane substrates, points to a much more homogeneous substrate at the droplet length scale.

Conclusions

In this paper, we have reported a new AFM technique for imaging liquid structures directly condensed onto solid surfaces by using the noncontact mode. The setup used achieves true noncontact profiling, thus ensuring a very low degree of sample perturbation compared to tapping mode, as shown by phase images. The wetting contact angle can be directly accessed from AFM topography, provided that instrumental artifacts, like tip−sample geometrical convolution and finite response time of the *Z* servo feedback, are correctly evaluated. The same method allows for spatial variations of the substrate wettability to be evidenced by recording nanoscale distortions of the liquid contact line and its hysteretical behavior. This is important to validate modern theories of capillary phenomena on a small scale and to better understand the microscopic origin of contact angle hysteresis.

By using this technique, we have studied the partial wetting of light alkanes on different types of methyl-terminated SAM. We have shown in particular that incomplete OTS monolayers are strongly heterogeneous at the micron scale, while complete ones are much more homogeneous as expected. Nevertheless, for the latter substrates, a noticeable reduction of the alkane contact angle is observed for droplet radii on the nanoscale. On the basis of theoretical estimations, we have concluded that this effect cannot be due only to a line tension arising in this case from purely dispersive solid−liquid interactions. More presumably, mesoscale substrate defects, which are intrinsic to the OTS self-assembly process, are strong enough to affect wetting whenever the droplet size become sufficiently small. Similar conclusions can be drawn in the case of alkyl monolayer assembled on silicon.

The wettability of dodecanethiol monolayers on gold is strongly affected by the roughness of the metallic substrate, a feature which can be largely reduced by modifying the preparation of gold layers. Although structurally unstable when in contact with the liquid alkanes, hexatriacontane substrates prove to be more homogeneous at the mesoscale.

The ensemble of these results demonstrate that the line tension arising from purely dispersive interactions is negligibly small for contact line curvatures less that some $10\,\mu m^{-1}$ with basically no influence on the wettability of actual microfluidic devices. Much more important are spatial gradients of surface wettability, which can be difficult to control at the nanometer scale. Finally, the AFM proves a viable probe for testing the functionality of open micro- and nanofluidic systems.

Acknowledgment. We thank J.P. Bourgoin and L. Patrone for providing a sample of distilled 1-dodecanethiol and P. Orfila for the vacuum gold deposition. A.C. thanks L. Pham Van for his valuable help regarding some technical AFM issues.

LA051419B